

Highly Reversible Lithium Storage in *Bacillus subtilis*-Directed Porous Co_3O_4 Nanostructures

Hyun-Woo Shim, Yun-Ho Jin, Seung-Deok Seo, Seung-Hun Lee, and Dong-Wan Kim*

Department of Materials Science and Engineering, Ajou University, Suwon 443-749, Korea

The template technique is versatile for the construction of advanced materials with controlled nano/microstructures and desired functions.^{1–4} To date, various hard templates with pre-formed porous or channel structures, such as anodized alumina membranes and MCM-41 silica, have been explored for the synthesis of nanorods and nanotubes.^{5,6} Other soft templates, such as surfactants and block copolymers, function as structure-directing agents that assist in the assembly of the reacting species. These templates offer benefits in terms of designing spherelike, wirelike, and porous nanostructures.^{7–10} More recently, one type of soft templates, biological templates (bacterium, DNA, virus particles, etc.), has been used to deposit nanoparticles and produce unique nanostructures.^{11–14} Comparatively, bacteria could be promising in the generation of a variety of unique inorganic structures on the micro- or even nanoscopic level, through the combination of traditional chemical techniques without stringent genetic engineering.^{7,11,15–19} These structures could possibly be used for the facile, large-scale production of functional materials.

Herein, rod- or tube-shaped metal oxide nanostructures were synthesized using *Bacillus subtilis* templates. *Bacillus subtilis* is one of the extensively studied Gram-positive bacterium with a thick, multilayered peptidoglycan sacculus that is decorated with proteins, teichoic acids, and polysaccharides, which are surrounded by an outer shell of proteins that are packed in a paracrystalline layer (S-layer) in some species.^{20,21} An aqueous electroless deposition procedure was demonstrated utilizing the metal-binding properties of this bacte-

ABSTRACT In this work, a simple, high-yield biomineralization process is reported for cobalt oxide nanostructures using Gram-positive bacteria, *Bacillus subtilis*, as the soft templates. Rod-type cobalt oxide is prepared at room temperature through an electrostatic interaction between the functional surface structures of the bacteria and the cobalt ions in an aqueous solution. Additionally, porous Co_3O_4 hollow rods are formed through a subsequent heat treatment at 300 °C. These rods have a high surface area and exhibited an excellent electrochemical performance for rechargeable Li-ion batteries. This facile, inexpensive, and environmentally benign synthesis for transition metal oxides with unique nanostructures can be used for several practical applications, such as batteries, catalysts, sensors, and supercapacitors.

KEYWORDS: *Bacillus subtilis* · soft template · cobalt oxide · nanostructures · lithium-ion batteries

rial surface in order to fabricate cobalt oxide nanostructures that retained the shape of the bacterial template morphology. p-Type semiconductor cobalt oxide was selected as the functional inorganic material because it has intensively been studied in catalysts, solid-state sensors, electrochromic devices, and pigments.^{22–25} Recently, cobalt oxides have also received special attention for their applications in high-capacity Li-ion battery electrodes.^{17,26–30} In this work, organic/inorganic hybrid bacteria/cobalt oxide rods and hollow cobalt oxide rods with a high surface area were systematically fabricated. Furthermore, we investigated the lithium storage properties of these nanostructured materials.

RESULTS AND DISCUSSION

Bacteria-Templated Synthesis. Figure 1a schematically illustrates the *Bacillus subtilis*-mediated biosynthetic process of the cobalt oxide nanostructures: (i) the cultured bacteria biotemplates, (ii) the bacteria/metal oxide composite rods that were synthesized through the binding/reduction of the metal ions on the bacterial surface and the spontaneous oxidation at room temperature,

*Address correspondence to dwkim@ajou.ac.kr.

Received for review August 25, 2010 and accepted December 07, 2010.

Published online December 14, 2010. 10.1021/nn1021605

© 2011 American Chemical Society

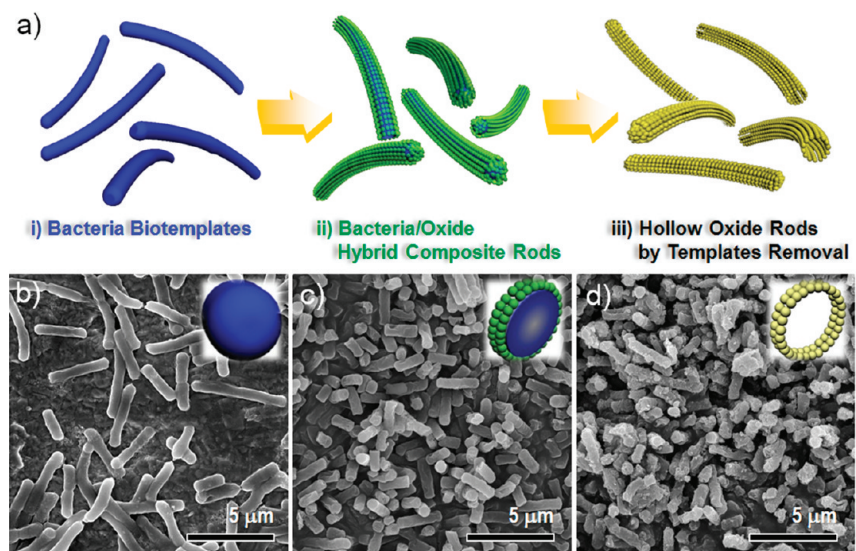


Figure 1. (a) Schematic diagram of the bacteria-templated synthesis of the oxide nanostructures. Typical FESEM images of (b) the pure bacteria, (c) the bacteria/cobalt oxide rods, and (d) the hollow cobalt oxide rods. The insets depict the cross section of each sample.

and (iii) the highly porous metal oxide tubes that were heat-treated at 300 °C. The field-emission scanning electron microscopy (FESEM) images of the typical structures were taken after each step and are depicted in Figure 1b–d. *Bacillus subtilis* is a rod-shaped bacterium with an average diameter of ~500 nm and a length of 2–5 μ m, as shown in Figure 1b. The uniform deposition of cobalt oxide onto the bacterial surfaces without any further functionalization led to the formation of the bacteria/cobalt oxide hybrid systems (Figure 1c).

The *Bacillus subtilis* cell wall is composed of a thick, multilayered peptidoglycan sheath outside of the plasma membrane. The phosphate groups in the form of phosphodiesters of teichoic and lipoteichoic acids that were linked to and embedded in the peptidoglycan contributed to the highly negative surface charge (Figure 2).^{21,31} Indeed, the well-dispersed bacterial suspension exhibited a high negative zeta-potential of -46 mV . Wall teichoic acid chains and carbonyl groups of peptidoglycan were believed to bind the positive Co^{2+} ions through an electrostatic interaction.^{32,33} The hybrid core/shell bacteria/cobalt oxide rods were synthesized after the subsequent reduction by NaBH_4 and

the spontaneous oxidation in an aqueous suspension. In order to characterize a possible reaction of bacterial surface with Co^{2+} ions, a UV–visible absorption spectra of solution were obtained with increasing reaction time at room temperature. A clear absorption peak around 500 nm is observed in pure $\text{CoCl}_2 \cdot 6\text{H}_2\text{O}$ solution and then became significantly weaker after adding bacterial solution (Figure S1, Supporting Information). In addition, the solution does not have any noticeable absorption after subsequent addition of NaBH_4 solution, which indicates the formation of Co^0 nanometals by the reduction reaction as reported in UV–visible spectra of cobalt nanoparticles.^{34,35} This subsequent reduction of Co^{2+} ions by NaBH_4 was clearly evidenced by the systematic color change from pink to a black, as shown in Figure S1. Furthermore, the black coloration of solution changed to dark yellow by the spontaneous oxidation in aqueous solution with the increase of reaction time.

Most of the rods had a closed end, but some open-ended rods and hollow-structured rods also existed in the broken region probably because of the cellular fragment release during the synthetic process (Figure 3). Furthermore, these hybrid rods were calcined at 300 °C for 12 h in air to design the complete cobalt oxide hollow rods or tubes with a high surface area. The overall rod-shaped morphology was clearly retained after the core bacteria removal process. The expected cross sections of each sample are illustrated in the insets of Figure 1b,c.

Microstructure and Phase Analyses. The microstructure was further examined using transmission electron microscopy (TEM) and selected area electron diffraction (SAED). Compared to the clear surface of the original *Bacillus subtilis* templates (Figure 4a), the nano-clusters covered the overall bacteria surfaces (Figure

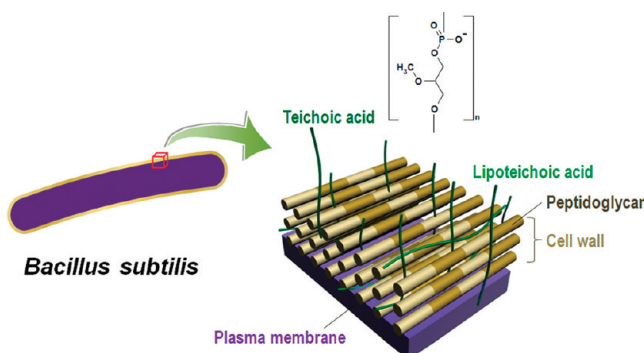


Figure 2. Simplified illustration of the cell wall of *Bacillus subtilis*, which shows the teichoic/lipoteichoic acid brushes on the bacterial surface.

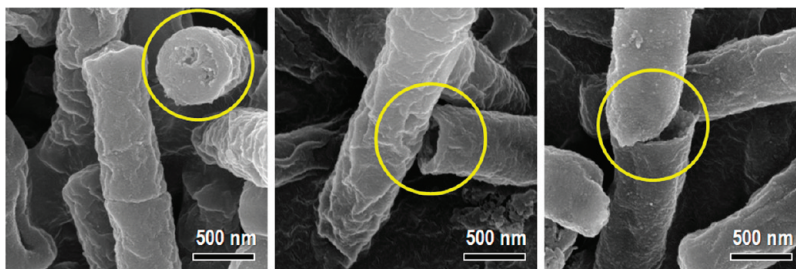


Figure 3. Representative FESEM images of the close-ended, open-ended, and broken hollow rods.

4b). These nanoclusters (~ 2 to 5 nm in diameter), which were crystallized onto the surfaces, corresponded to the crystal structure of Co(II)O based on high-resolution TEM (HRTEM) and the SAED pattern (insets in Figure 4b).

The focused ion beam (FIB) lift-out technique was used to obtain the cross-sectional information of the hybrid bacteria/cobalt oxide rods. A weaker contrast region surrounded by a strong dark region was observed, revealing the clear core–shell structure in Figure 4c. The line-scan energy-dispersive spectroscopy (EDS) analysis confirmed the local composition of the core (bacteria)–shell (cobalt oxide) structure. The thickness of shell was estimated to be 20 – 50 nm. Notably, the thickness of the shell (i.e., the amount of cobalt oxide that was coated onto the bacteria) was easily controlled by the synthetic conditions, especially the concentrations of the Co^{2+} ions and NaBH_4 (Figure 5).³⁶ We found that thicker cobalt oxide rods were produced with an increase in concentration of NaBH_4 when the concentration of Co^{2+} ions was held constant (Figures S2 and S3, Supporting Information).

Furthermore, the FIB-TEM-EDS analyses of the other hybrid rods were conducted using the other samples (Figure S4). The incomplete circular shape of the hybrid rods was due to the deposition of the Pt strap onto the rods and the Ga^+ beam milling processes (Figure S4a,b). On the basis of the intensity profiles of the elements (Co, C, O, and Pt) along the line on the bacteria/cobalt oxide rods, the high C signal in the core region and high Co and O signals in the shell region (Figure S4c,d) supported the formation of the core–shell heterostructure.

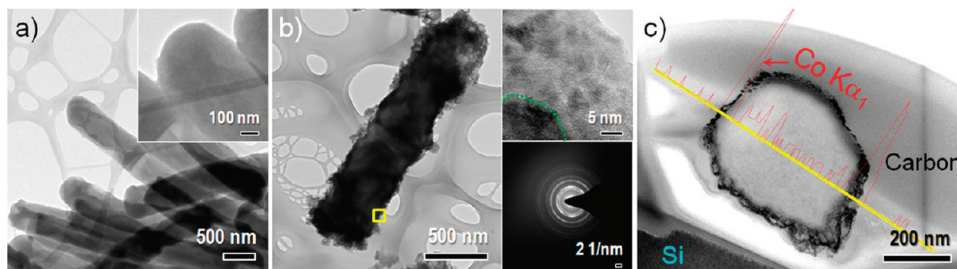


Figure 4. (a) TEM image of the pure *Bacillus subtilis* templates. The inset shows a magnified image of the cell end part. (b) TEM image of an individual bacteria/cobalt oxide composite rod. The top right and bottom right insets show the HRTEM images of the enlarged view of the interface between the core and the shell and the SAED pattern that confirmed the CoO -like crystal structure of the shell. (c) Cross-section TEM image of the bacteria/cobalt oxide composite rod through an FIB manipulation process. The EDS intensity profile of the Co element along the yellow line.

Figure 6a,b shows the typical TEM images of the cobalt oxide rods that were heat-treated for 12 h at 200 and 300 °C, respectively. During the core removal process with the heat treatment, the microstructure retained the original morphology of the bacterium. The rod shape did not significantly collapse, even though the lengths of the rods were shorter. Furthermore, the rods were irregularly shrunken, and their surface was relatively rougher, possibly because of the core release. The quantitative analysis using TEM-EDS (Figure S5) and the inductively coupled plasma mass spectrometry analysis indicated that the pure *Bacillus subtilis* bacterium had a typical elemental composition for organic material, and the amount of the inorganic residues (mainly P and K) was negligible. From the thermogravimetric analysis (TGA), the as-prepared bacteria/cobalt oxide hybrids were completely decomposed during the heat treatment at 300 °C for 12 h (Figure S6). The total weight loss corresponded to $\sim 60\%$. Therefore, after the thermal treatment at 300 °C, the powder corresponded to complete inorganic cobalt oxides with hollow rod shapes (bottom left inset of Figure 6b and Figure S7). The SAED pattern corresponded to the polycrystalline cubic spinel Co_3O_4 (top right inset of Figure 6b and Figure S8).

The crystallographic structure was also analyzed using the X-ray powder diffraction (XRD) patterns that were taken from these powders in Figure 6c. All of the peaks were perfectly indexed to Co_3O_4 (JCPDS card No. 42-1467, space group $Fd\bar{3}m$), as expected. All of the prominent Raman peaks also corresponded to the E_g (466 cm^{-1}), F_{2g} (512 and 621 cm^{-1}), A_{1g} (668 cm^{-1}) modes of the Co_3O_4 crystalline phase (inset of Figure

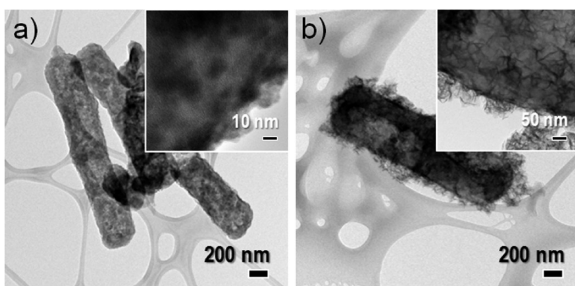


Figure 5. Typical TEM images of the bacteria/cobalt oxide composite rods that were prepared under different synthetic conditions: (a) 100 mL of 1 mM $\text{CoCl}_2 \cdot 6\text{H}_2\text{O}$ and 1 mL of 100 mM NaBH_4 , (b) 200 mL of 50 mM $\text{CoCl}_2 \cdot 6\text{H}_2\text{O}$ and 300 mL of 50 mM NaBH_4 .

6c), which was consistent with the previous investigations.³⁷ Additionally, the mean crystallite size was estimated to be 6.6 nm from the calculation of the half-width of the XRD peak of the Co_3O_4 (311) plane using Scherrer's equation. These results suggested that the crystallinity of cobalt oxide improved, and the primary crystallites grew, while maintaining the nanotextural nature of the samples after the thermal treatment.

The thermal process for the removal of the bacteria as the sacrificial template could affect the surface area and the porosity of the cobalt oxide powders. Figure 6d provides the nitrogen adsorption–desorption iso-

therms of the pure bacteria and the hollow Co_3O_4 rods that were heat-treated at 300 °C. The Brunauer–Emmett–Teller (BET) surface areas were estimated to be 5.1 and 73.3 $\text{m}^2 \text{ g}^{-1}$, respectively. Although the as-prepared bacteria/cobalt oxide hybrid rods had a surface area of 11.2 $\text{m}^2 \text{ g}^{-1}$, the surface area of the Co_3O_4 rods was much larger after the thermal treatment. Additionally, the clear hysteresis loop and the pore size distribution that was calculated using the Barrett–Joyner–Halenda (BJH) method (inset of Figure 6d) indicated the mesoporosity of the Co_3O_4 rods. Thus, the hollow-rod-type porous Co_3O_4 nanostructures with a high surface area can be prepared using the thermal bacteria removal process.

Electrochemical Properties of Cobalt Oxide Nanostructures.

Nanostructured electrode materials with large surface areas have multiple advantages with respect to the performance of Li-ion batteries by providing shorter path lengths for both the electronic and the Li ionic transport, a higher electrode/electrolyte contact area, and a better accommodation of the strain of the Li-ion insertion/extraction.^{38–40} Because of the capacity limitation (theoretical capacity of 372 mAh g^{-1}) in commercial graphite-based anodes on intercalation/deintercalation reactions, great effort has been applied to the nanostructuring of transition metal oxides (that is, M_xO_y , where M is Co, Ni, Cu, or Fe) because nanostructured

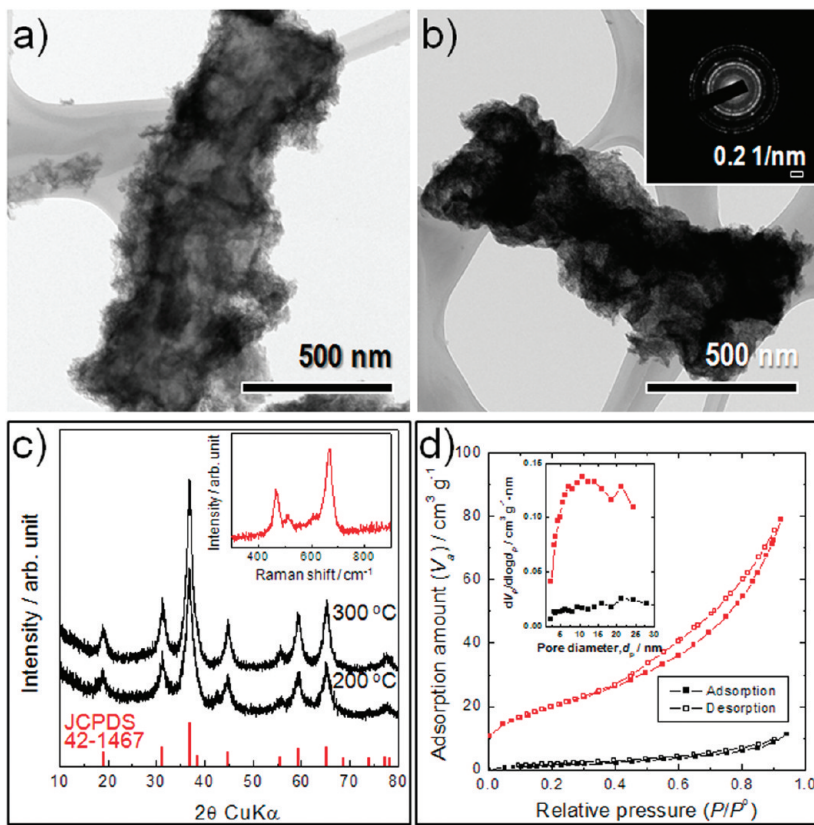


Figure 6. TEM images of the Co_3O_4 rods that were calcined at (a) 200 °C and (b) 300 °C. The top right and bottom left insets in (b) indicate the typical SAED pattern and FESEM image showing the hollow nature, respectively. (c) XRD patterns of the Co_3O_4 rods that were calcined at 200 and 300 °C. The inset shows the room temperature Raman spectrum of the Co_3O_4 rods that were calcined at 300 °C. (d) Nitrogen adsorption–desorption isotherms along with the corresponding pore size distributions (inset) of the pure bacteria and the Co_3O_4 rods that were calcined at 300 °C.

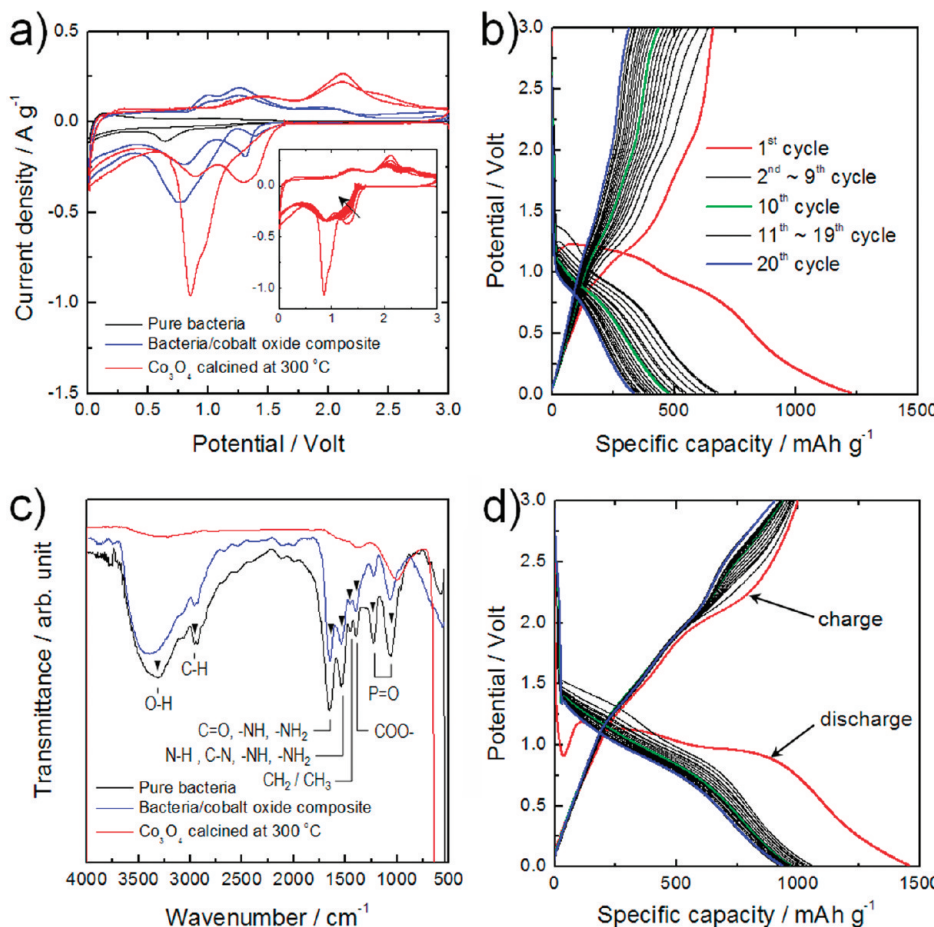


Figure 7. (a) Cyclic voltammetries of the pure bacteria, the bacteria/cobalt oxide rods, and the hollow Co_3O_4 rods that were calcined at 300 °C for the first two cycles. The inset shows the variation in the CV profiles of the hollow Co_3O_4 rods that were calcined at 300 °C for 10 cycles. (b) Charging–discharging curves of the bacteria/cobalt oxide composite rods. (c) FT-IR spectra of the pure bacteria, the bacteria/cobalt oxide rods, and the hollow Co_3O_4 rods that were calcined at 300 °C. (d) Charging–discharging curves of the hollow Co_3O_4 rods that were calcined at 300 °C.

transition metal oxides can deliver much higher capacity than graphite using their conversion reaction ($\text{M}_x\text{O}_y + ne^- + n\text{Li}^+ \leftrightarrow x\text{M}^0 + \text{Li}_n\text{O}_y$).^{25–29} Moreover, biologically derived components have been recently used to produce high surface area nanostructured materials for the battery electrodes.^{14,17}

The electrochemical activity of bacteria-directed nanostructured samples was evaluated using cyclic voltammetry (CV). Figure 7a presents the CV profiles of the pure bacteria, the bacteria/cobalt oxide composite rods, and the hollow Co_3O_4 rods after the first two cycles at a scan rate of 0.1 mV s⁻¹ from 0.01 to 3.0 V. For the pure bacteria, the trace of an irreversible reduction peak appeared at ~0.65 V for the first cycle, but no further redox peaks were observed upon subsequent charging/discharging, indicating that the lithiation reaction was negligible for the bacteria. The redox peaks of the bacteria/cobalt oxide composite rods shifted to a lower voltage, compared to the hollow Co_3O_4 rods, possibly because of the different species of cobalt oxides (CoO and Co_3O_4 , respectively) along with the different lithium conversion reactions ($\text{CoO} + 2\text{Li} \rightleftharpoons \text{Co} + \text{Li}_2\text{O}$ and $\text{Co}_3\text{O}_4 + 8\text{Li} \rightleftharpoons 3\text{Co} + 4\text{Li}_2\text{O}$). Furthermore, the CV pro-

files of the hollow Co_3O_4 rods were almost identical to the Co_3O_4 nanostructures (inset of Figure 7a).^{17,41}

Figure 7b shows the typical voltage/specific capacity curves at a rate of 240 mA g⁻¹ in the bacteria/cobalt oxide composite rods. The first discharge and charge capacities were 1225 and 660 mAh g⁻¹, respectively. Considering the amount of inactive bacteria (~60 wt %), the first charge capacity was considerably high. However, the Coulombic efficiency of 54% was poor during the first cycle, and the reversible capacity significantly faded to 310 mAh g⁻¹ after 20 cycles. The observed infrared bands for the bacteria in Figures 7c and S9 corresponded to the presence of the functional groups from the macromolecules.⁴² These assigned signals were also observed in the bacteria/cobalt oxide composite rods. Although the exact electrochemical reaction must be further investigated, this inferior performance could possibly be attributed to the undesirable electrode–electrolyte reaction and the poor internal electronic conductivity that was induced by the contributions from the considerable amount of functional organic species. These organic groups almost completely disappeared after the thermal bacteria re-

moval process at 300 °C in the hollow Co_3O_4 rods. Therefore, the Coulombic efficiency was remarkably improved (69%) under the same electrochemical evaluation conditions (at a rate of 240 mA g⁻¹ (0.2C, based on the theoretical capacity of 890 mAh g⁻¹ for Co_3O_4)). Furthermore, excellent reversible specific capacities of 1000, 936, and 903 mAh g⁻¹ were observed after 1, 10, and 20 cycles, respectively, indicating a better lithium storage capacity retention (Figure 7d). The porous nanostructures of the electrode materials can effectively accommodate the mechanical strain, thereby enhancing the cycle stability.^{27–30,43} As previously observed for the porous Co_3O_4 nanostructured electrodes, this enhanced electrochemical performance might be attributed to the porous/hollow structured Co_3O_4 rods with a high surface area.

METHODS

Bacteria Culture. The *Bacillus subtilis*-cotG bacterial cells were grown from a single colony in a liquid medium of the Luria–Bertani broth (LB broth, Sigma-Aldrich) including 50 mg/mL of chloramphenicol (Cm, Sigma-Aldrich) at 37 °C and 200 rpm in a shaking incubator. When the optical density (OD 600 nm) of the culture reached *ca.* 0.3–0.6, the culture was transferred into triangle flasks for subculturing. After subculturing for 5 h, the bacterial cells were centrifuged at 12 000 rpm for 10 min and resuspended in distilled water to adjust the optical density (OD 600 nm) to \sim 2.0.

Synthesis of the Cobalt Oxide Nanostructures. The cobalt oxide nanostructures were synthesized by adding the precursor solution and the reducing agent into the as-prepared bacterial suspension and stirring the mixture at 700 rpm and room temperature. First, 400 mL of the precursor solution, a 50 mM $\text{CoCl}_2 \cdot 6\text{H}_2\text{O}$ (99%, Sigma-Aldrich) aqueous solution, was injected into the bacterial suspension at a rate of 10 mL/min through a buret. After the mixture was stirred for 30 min, 200 mL of a 50 mM NaBH_4 (99%, Sigma-Aldrich) aqueous solution, as the reducing agent, was slowly poured into the mixture at a flow rate of 10 mL/min through the buret. Then the final mixture was robustly stirred for 24 h at room temperature. After the mixture was fully reacted, the mixture was centrifuged, and subsequently, the precipitate was collected. Then the precipitate was washed with distilled water several times and acetone and then dried at 60 °C in a vacuum oven for 6 h. The concentrations of Co ions and the reductant were systematically controlled in order to maintain a certain degree of control over the rod thickness.³⁶ The as-prepared bacteria/cobalt oxide composite rods were calcined at 200 and 300 °C for 12 h in air in order to produce the hollow cobalt oxide nanostructures.

Characterization. The concentration of the bacterial suspension was measured using UV–visible spectroscopy (model HP8453, Hewlett-Packard, USA). The crystal structures and functionality of the surface properties were analyzed using X-ray powder diffraction (XRD, model D/max-2500 V/PC, Rigaku Co., Japan), a Fourier transform infrared spectrometer (FT-IR, model 2000, Perkin-Elmer Inc., USA), and Raman spectroscopy (model T64000, Horiba Jovin Yvon, France). All of morphologies of the cobalt oxide nanostructures and the pure bacteria were investigated using a field-emission scanning electron microscope (FESEM, model Nova nanoSEM 200, FEI Co., USA) with an acceleration voltage of 10 kV and high-resolution transmission electron microscopy (HRTEM, model Tecnai G2 F30 S-Twin, FEI Co., USA) that was equipped with an energy-dispersive X-ray spectrometer (EDS, model EDAX, AMETEK Inc., USA). The cross-sectional images of the product were acquired using a transmission electron microscope, and the samples were fabricated using a focused ion beam (FIB, model Nova 600 NanoLab, FEI Co., USA). Additionally, the specific surface areas and the pore size distributions of the products were examined using the Brunauer–Emmett–Teller and Barrett–Joyner–Halenda (BET/

CONCLUSIONS

In summary, the bacteria/cobalt oxide hybrid composite rods were prepared using Gram-positive bacteria, *Bacillus subtilis*, as the soft templates without any further functionalization. The cobalt oxide nanoclusters with a diameter of \sim 2 to 5 nm were uniformly crystallized onto the bacterial surfaces through an electrostatic interaction between the functional surface structures of the bacteria and the cobalt ions. Furthermore, the porous, hollow Co_3O_4 rods with a high surface area of 73.3 m² g⁻¹ were designed using the thermal bacteria removal process. These Co_3O_4 nanostructures exhibited an enhanced Coulombic efficiency as well as an excellent reversible specific capacity of 903 mAh g⁻¹ after 20 cycles.

BJH, model Belsorp-mini II, BEL Japan Inc.) method along with a nitrogen adsorption/desorption process.

Evaluation of the Electrochemical Properties. A mixture that comprised 70 wt % active materials, 15 wt % Super P carbon black (MMM Carbon, Brussels, Belgium), and 15 wt % Kynar 2801 binder (PVdF-HFP) that was dissolved in a 1-methyl-2-pyrrolidinone (NMP) solvent was uniformly spread onto a Cu foil in order to prepare the positive electrodes of the cobalt oxide powders. Then the solvent was evaporated in a vacuum oven at 100 °C. A Swagelok-type cell was assembled in an Ar-filled glovebox in order to avoid contamination and oxidation. This cell was composed of a positive electrode, a Li metal foil as the negative electrode, and a separator film (Celgard 2400) that was saturated with a liquid electrolyte consisting of 1 M LiPF₆ that was dissolved in a ethylene carbonate and dimethyl carbonate (1:1 by volume, Techno Semichem Co., Ltd., Korea) solution. The cobalt oxide powders were electrochemically examined using the galvanostatic discharge/charge cycling method with a battery cycler (WBCS 3000, WonATech Co., Korea). Each cell was cycled over the voltage window of 0.01–3.0 V versus Li/Li⁺. The cyclic voltammetry analyses were carried out at a scanning rate of 0.1 mV s⁻¹.

Acknowledgment. This work was supported by the National Research Foundation of Korea (NRF) grant funded by the Korea government (MEST) (Nos. 2009-0082544 and 2010-0002533).

Supporting Information Available: UV–visible absorption spectra and digital camera images of solutions at each synthetic step, experimental conditions and the FESEM images of bacteria/cobalt oxide composite rods, FIB-TEM-EDS analyses of a bacteria/cobalt oxide composite rod, TEM-EDS analysis of pure bacteria, TGA result of bacteria/cobalt oxide composite rods, FESEM images of the Co_3O_4 rods that were calcined at 300 °C, enlarged SAED pattern of the inset of Figure 6b, and enlarged FT-IR spectra of Figure 7c. This material is available free of charge via the Internet at <http://pubs.acs.org>.

REFERENCES AND NOTES

- Cheng, F.; Tao, Z.; Liang, J.; Chen, J. Template-Directed Materials for Rechargeable Lithium-Ion Batteries. *Chem. Mater.* **2008**, *20*, 667–681.
- Lin, H. P.; Mou, C. Y. Structural and Morphological Control of Cationic Surfactant-Templated Mesoporous Silica. *Acc. Chem. Res.* **2002**, *35*, 927–935.
- Schüth, F. Endo- and Exotemplating To Create High-Surface-Area Inorganic Materials. *Angew. Chem., Int. Ed.* **2003**, *42*, 3604–3622.
- van Bommel, K. J.; Friggeri, A.; Shinkai, S. Organic Templates for the Generation of Inorganic Materials. *Angew. Chem., Int. Ed.* **2003**, *42*, 980–999.

5. Furneaux, R. C.; Rigby, W. R.; Davidson, A. P. The Formation of Controlled-Porosity Membranes from Anodically Oxidized Aluminium. *Nature* **1989**, *337*, 147–149.
6. Enzel, P.; Zoller, J. J.; Bein, T. Intrazeolite Assembly and Pyrolysis of Polyacrylonitrile. *J. Chem. Soc., Chem. Commun.* **1992**, *633*–635.
7. Zhou, H.; Fan, T.; Zhang, D.; Guo, Q.; Ogawa, H. Novel Bacteria-Templated Sonochemical Route for the *In Situ* One-Step Synthesis of ZnS Hollow Nanostructures. *Chem. Mater.* **2007**, *19*, 2144–2146.
8. Liu, J.; Bai, S.; Zhong, H.; Li, C.; Yang, Q. Tunable Assembly of Organosilica Hollow Nanospheres. *J. Phys. Chem. C* **2010**, *114*, 953–961.
9. Du, C.; Yun, J.; Dumas, R. K.; Yuan, X.; Liu, K.; Browning, N. D.; Pan, N. Three-Dimensionally Intercrossing Mn_3O_4 Nanowires. *Acta Mater.* **2008**, *56*, 3516–3522.
10. Polarz, S.; Antonietti, M. Porous Materials via Nanocasting Procedures: Innovative Materials and Learning about Soft-Matter Organization. *Chem. Commun.* **2002**, *2593*–2604.
11. Pollmann, K.; Raff, J.; Merroun, M.; Fahmy, K.; Selenska-Pobell, S. Metal Binding by Bacteria from Uranium Mining Waste Piles and Its Technological Applications. *Biotechnol. Adv.* **2006**, *24*, 58–68.
12. Hou, S.; Wang, J.; Martin, C. R. Template-Synthesized DNA Nanotubes. *J. Am. Chem. Soc.* **2005**, *127*, 8586–8587.
13. Flynn, C. E.; Lee, S.-W.; Peele, B. R.; Belcher, A. M. Viruses as Vehicles for Growth, Organization and Assembly of Materials. *Acta Mater.* **2003**, *51*, 5867–5880.
14. Royston, E.; Ghosh, A.; Kofinas, P.; Harris, M. T.; Culver, J. N. Self-Assmbly of Virus-Structured High Surface Area Nanomaterials and Their Application as Battery Electrodes. *Langmuir* **2008**, *24*, 906–912.
15. Bhardwaj, A. A.; Parikh, R. Y.; Baidakova, M.; Jouen, S.; Hannoyer, B.; Enoki, T.; Prasad, B. L.; Shouche, Y. S.; Ogale, S.; Sastry, M. Bacteria-Mediated Precursor-Dependent Biosynthesis of Superparamagnetic Iron Oxide and Iron Sulfide Nanoparticles. *Langmuir* **2008**, *24*, 5787–5794.
16. Berry, V.; Rangaswamy, S.; Saraf, R. F. Highly Selective, Electrically Conductive Monolayer of Nanoparticles on Live Bacteria. *Nano Lett.* **2004**, *4*, 939–942.
17. Nam, K. T.; Kim, D. W.; Yoo, P. J.; Chiang, C. Y.; Meethong, N.; Hammond, P. T.; Chiang, Y. M.; Belcher, A. M. Virus-Enabled Synthesis and Assembly of Nanowires for Lithium Ion Battery Electrodes. *Science* **2006**, *312*, 885–888.
18. Lee, Y. J.; Yi, H.; Kim, W. J.; Kang, K.; Yun, D. S.; Strano, M. S.; Ceder, G.; Belcher, A. M. Fabricating Genetically Engineered High-Power Lithium-Ion Batteries Using Multiple Virus Genes. *Science* **2009**, *324*, 1051–1055.
19. Ahmad, G.; Dickerson, M. B.; Cai, Y.; Jones, S. E.; Ernst, E. M.; Vernon, J. P.; Haluska, M. S.; Fang, Y.; Wang, J.; Subramanyam, G.; et al. Rapid Bioenabled Formation of Ferroelectric $BaTiO_3$ at Room Temperature from an Aqueous Salt Solution at Near Neutral pH. *J. Am. Chem. Soc.* **2008**, *130*, 4–5.
20. Delcour, J.; Ferain, T.; Deghorain, M.; Palumbo, E.; Hols, P. The Biosynthesis and Functionality of the Cell-Wall of Lactic Acid Bacteria. *Antonie Van Leeuwenhoek* **1999**, *76*, 159–184.
21. Ahimou, F.; Boonaert, C. J.; Adriaensen, Y.; Jacques, P.; Thonart, P.; Paquot, M.; Rouxhet, P. G. XPS Analysis of Chemical Functions at the Surface of *Bacillus subtilis*. *J. Colloid Interface Sci.* **2007**, *309*, 49–55.
22. Ando, M.; Kobayashi, T.; Iijima, S.; Haruta, M. Optical Recognition of CO and H_2 by Use of Gas-Sensitive Co_3O_4 Composite Films. *J. Mater. Chem.* **1997**, *7*, 1779–1783.
23. Patil, D.; Patil, P.; Subramanian, V.; Joy, P. A.; Potdar, H. S. Highly Sensitive and Fast Responding CO Sensor Based on Co_3O_4 Nanorods. *Talanta* **2010**, *81*, 37–43.
24. Selvaraj, M.; Palraj, S.; Maruthan, K.; Venkatachari, G. Physico-Chemical Properties of Ceramic Pigments for High-Temperature Application. *Prog. Org. Coat.* **2008**, *62*, 326–330.
25. Švegl, F.; Orel, B.; Hutchins, M. G.; Kalcher, K. Structural and Spectroelectrochemical Investigations of Sol–Gel Derived Electrochromic Spinel Co_3O_4 Films. *J. Electrochem. Soc.* **1996**, *143*, 1532–1539.
26. Poizot, P.; Laruelle, S.; Gruegeon, S.; Dupont, L.; Tarascon, J. M. Nano-Sized Transition-Metal Oxides as Negative-Electrode Materials for Lithium-Ion Batteries. *Nature* **2000**, *407*, 496–499.
27. Lou, X. W.; Deng, D.; Lee, J. Y.; Archer, L. A. Thermal Formation of Mesoporous Single-Crystal Co_3O_4 Nano-Needles and Their Lithium Storage Properties. *J. Mater. Chem.* **2008**, *18*, 4397–4401.
28. Zhan, F.; Geng, B.; Guo, Y. Porous Co_3O_4 Nanosheets with Extraordinarily High Discharge Capacity for Lithium Batteries. *Chem.—Eur. J.* **2009**, *15*, 6169–6174.
29. Tian, L.; Zou, H.; Fu, J.; Yang, X.; Wang, Y.; Guo, H.; Fu, X.; Liang, C.; Wu, M.; Shen, P. K.; et al. Topotactic Conversion Route to Mesoporous Quasi-Single-Crystalline Co_3O_4 Nanobelts with Optimizable Electrochemical Performance. *Adv. Funct. Mater.* **2010**, *20*, 617–623.
30. Li, C.; Yin, X.; Chen, L.; Li, Q.; Wang, T. Synthesis of Cobalt Ion-Based Coordination Polymer Nanowires and Their Conversion into Porous Co_3O_4 Nanowires with Good Lithium Storage Properties. *Chem.—Eur. J.* **2010**, *16*, 5215–5221.
31. Tortora, G. J.; Funke, B. R.; Case, C. L. *Microbiology: An Introduction* (International Edition), 10th ed. In *Functional Anatomy of Prokaryotic and Eukaryotic Cells*; Pearson–Benjamin Cummings Publishing, 2009.
32. Berry, V.; Gole, A.; Kundu, S.; Murphy, C. J.; Saraf, R. F. Deposition of CTAB-Terminated Nanorods on Bacteria To Form Highly Conducting Hybrid Systems. *J. Am. Chem. Soc.* **2005**, *127*, 17600–17601.
33. Erschov, B. G.; Sukhov, N. L.; Janata, E. Formation, Absorption Spectrum, and Chemical Reactions of Nanosized Colloidal Cobalt in Aqueous Solution. *J. Phys. Chem. B* **2000**, *104*, 6138–6142.
34. Kern, T.; Giffard, M.; Hediger, S.; Amoroso, A.; Giustini, C.; Bui, N. K.; Joris, B.; Bougault, C.; Vollmer, W.; Simorre, J. P. Dynamics Characterization of Fully Hydrated Bacterial Cell Walls by Solid-State NMR: Evidence for Cooperative Binding of Metal Ions. *J. Am. Chem. Soc.* **2010**, *132*, 10911–10919.
35. Bala, T.; Arumugam, S. K.; Pasricha, R.; Prasad, B. L. V.; Sastry, M. Foam-Based Synthesis of Cobalt Nanoparticles and Their Subsequent Conversion to $Co_{core}Ag_{shell}$ Nanoparticles by a Simple Transmetalation Reaction. *J. Mater. Chem.* **2004**, *14*, 1057–1061.
36. Shim, H. W.; Lee, C. S.; Kim, D. W. Bacteria-Mediated Synthesis of Free-Standing Cobalt Oxide Rods. *J. Nanosci. Nanotechnol.* **2010**, *10*, 1129–1134.
37. Tang, C.-W.; Wang, C.-B.; Chien, S.-H. Characterization of Cobalt Oxides Studied by FT-IR, Raman, TPR and TG-MS. *Thermochim. Acta* **2008**, *473*, 68–73.
38. Aricò, A. S.; Bruce, P.; Scrosati, B.; Tarascon, J. M.; van Schalkwijk, W. Nanostructured Materials for Advanced Energy Conversion and Storage Devices. *Nat. Mater.* **2005**, *4*, 366–377.
39. Bruce, P. G.; Scrosati, B.; Tarascon, J. M. Nanomaterials for Rechargeable Lithium Batteries. *Angew. Chem., Int. Ed.* **2008**, *47*, 2930–2946.
40. Kim, D. W.; Ko, Y. D.; Park, J. G.; Kim, B. K. Formation of Lithium-Driven Active/Inactive Nanocomposite Electrodes Based on $Ca_3Co_4O_9$ Nanoplates. *Angew. Chem., Int. Ed.* **2007**, *46*, 6654–6657.
41. Li, F.; Zou, Q.-Q.; Xia, Y.-Y. CoO-Loaded Graphitable Carbon Hollow Spheres as Anode Materials for Lithium-Ion Battery. *J. Power Sources* **2008**, *177*, 546–552.
42. Ojeda, J. J.; Romero-Gonzalez, M. E.; Bachmann, R. T.; Edyvean, R. G.; Banwart, S. A. Characterization of the Cell Surface and Cell Wall Chemistry of Drinking Water Bacteria by Combining XPS, FTIR Spectroscopy, Modeling, and Potentiometric Titrations. *Langmuir* **2008**, *24*, 4032–4040.
43. Zheng, J.; Liu, J.; Lv, D.; Kuang, Q.; Jiang, Z.; Xie, Z.; Huang, R.; Zheng, L. A Facile Synthesis of Flower-like Co_3O_4 Porous Spheres for the Lithium-Ion Battery Electrode. *J. Solid State Chem.* **2010**, *18*, 600–605.